# Associative detachment of $H^- + H \rightarrow H_2 + e^-$

K. A. Miller,[1] H. Bruhns,[1,*] J. Eliášek,[2] M. Čížek,[2] H. Kreckel,[1,†] X. Urbain,[3] and D. W. Savin[1]

[1]*Columbia Astrophysics Laboratory, Columbia University, New York, New York 10027, USA*

[2]*Institute of Theoretical Physics, Faculty of Mathematics and Physics, Charles University Prague, CZ-180 00 Praha 8, Czech Republic*

[3]*Institute of Condensed Matter and Nanosciences, Université Catholique de Louvain, B-1348 Louvain-la-Neuve, Belgium*

Using a merged-beams apparatus, we have measured the associative detachment (AD) reaction of $H^- + H \rightarrow H_2 + e^-$ for relative collision energies up to $E_r \leqslant 4.83$ eV. These data extend above the 1-eV limit of our earlier results. We have also updated our previous theoretical work to account for AD via the repulsive $^2\Sigma_g^+$ $H_2^-$ potential energy surface and for the effects at $E_r \geqslant 0.76$ eV on the experimental results due to the formation of long-lived $H_2$ resonances lying above the H + H separated atoms limit. Merging both experimental data sets, our results are in good agreement with our new theoretical calculations and confirm the prediction that this reaction essentially turns off for $E_r \gtrsim 2$ eV. Similar behavior has been predicted for the formation of protonium from collisions of antiprotons and hydrogen atoms.

PACS number(s): 34.50.Lf, 52.20.Hv, 95.30.Ft, 97.10.Bt

## I. INTRODUCTION

One of the simplest molecular formation reactions is associative detachment (AD) via

$$H^- + H \rightarrow H_2 + e^-. \tag{1}$$
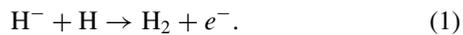
This reaction is of interest for fundamental atomic and molecular physics and also because it plays an important role in protogalactic and first star formation in the early universe [1–3]. Two groups have recently reported measurements of this reaction. Martinez *et al.* [4] measured the thermal rate coefficient at 300 K using a flowing afterglow technique. Our group has measured this reaction over a collision energy range from 4 meV to 1 eV using a merged-beams method [3,5,6]. Our results lie $2.2 \pm 0.9$ times above those of [4]. The quoted uncertainty represents the quadrature sum of the estimated total experimental $1\sigma$ confidence level for each measurement. We have also taken into account minor corrections to our earlier data, which are described below.

In [6] we hypothesized that this discrepancy is due to an error in the measured rate coefficient of [7] for

$$H + Cl^- \rightarrow HCl + e^-, \tag{2}$$
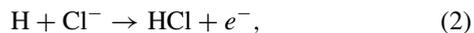
which [4] used to determine their neutral H number density and thereby normalize their results. Our apparatus is not configured to study reaction (2) and test this hypothesis, but we have been able to extend our measurements of reaction (1) to higher energies and thereby provide additional benchmarks for theory. We have also investigated and ruled out several possible sources of systematic errors in our previous experimental results. Additionally, we have more carefully considered the pressure dependence of our detection method. Last, we have updated our previous theoretical results of [3,8] to account for AD via the repulsive $^2\Sigma_g^+$ $H_2^-$ state and for the effects at $E_r \geqslant 0.76$ eV on the experimental results due to the formation

of long-lived $H_2$ resonances lying above the H + H separated atoms limit.

The rest of the paper is organized as follows: Sec. II describes the experimental method and the various modifications performed for this work. Section III discusses the experimental uncertainties. Our new theoretical calculations are briefly described in Sec. IV. In Sec. V we present our results and compare them to theory. A discussion of our results is given in Sec. VI and a short summary in Sec. VII.

## II. EXPERIMENT

Here we briefly describe the experiment and the changes relevant to our new results. Further details about the apparatus and experimental method can be found in [3,5,6].

### A. Method

We begin by extracting $H^-$ from a duoplasmatron source and forming a beam with an energy of $E_{H^-} = -e(U_s + U_f/2)$. Here $e$ is the unit charge, $U_s \approx -10$ kV is the nominal source voltage, and $U_f$ is a small correction voltage, which is defined below. Using standard ion-optical elements, we shape, steer, and direct the beam into a photodetachment chamber that houses a floating cell biased to a potential $U_f$. The anion energy inside the floating cell is $E_{H^-} = -e(U_s + U_f/2) + eU_f$. Near the center of the floating cell, we cross the anions with an infrared laser and convert a portion of the $H^-$ beam into a beam of ground-state H atoms of energy $E_H = -e(U_s - U_f/2)$. The resulting merged beams exit the floating cell, whereupon the $H^-$ beam returns to its initial energy, while the H beam energy remains unchanged. The beam-beam interaction energy is controlled by varying $U_f$.

Shortly after leaving the photodetachment chamber, the two beams enter an interaction region of length $L$. Two beam profile monitors (BPMs) are used to determine the beam-beam overlap $\langle \Omega(z) \rangle$ within the interaction region, where the $z$ axis is defined by the bulk velocity vectors of the copropagating beams. We also use the BPMs to verify the alignment of the

---

*Present address: Inficon GmbH, D-50968 Cologne, Germany.

†Present address: Department of Chemistry, University of Illinois, 600 South Mathews Avenue, Urbana, Illinois 61801, USA.

beam axes. The relative energy $E_r$ between the beams depends, in part, on this alignment and is given by [9] as

$$E_r = \mu \left( \frac{E_{H^-}}{m_{H^-}} + \frac{E_H}{m_H} - 2\sqrt{\frac{E_{H^-} E_H}{m_{H^-} m_H}} \cos\theta \right). \quad (3)$$

Here $\mu = m_{H^-} m_H / (m_{H^-} + m_H)$ is the reduced mass of the colliding system, $m_{H^-}$ and $m_H$ are the masses of the H$^-$ and H, respectively, and $\theta$ is the angle of intersection. $E_r$ is controlled by varying $U_f$. This merged-beams approach allows us to reach collision energies on the order of a few meV, limited only by the alignment of the beams, the spread in collision angles between the two beams, and the energy spread of each beam. We used geometrical simulations [3,5,6] to determine the average collision energy $\langle E_r \rangle$ versus $U_f$, taking into account the spreads in beam energies and angles.

Both beams are chopped out of phase in order to extract the signal H$_2$ generated in the interaction region from various backgrounds. Any H$_2$ formed in the interaction region has an energy of $E_{H_2} = E_{H^-} + E_H = -2eU_s = 20$ keV, neglecting the $\lesssim 3.7$ eV kinetic energy of the detached electron and the similarly small internal energy of the H$_2$ formed. At the end of this region, an electrostatic quadrupole deflector is used to direct the H$^-$ into a Faraday cup where the current $I_{H^-}$ is read and recorded. The parent H and daughter H$_2$ beams continue on into a gas cell kept at a helium pressure of $2 \times 10^{-4}$ Torr for most measurements. Inside the cell a fraction of the H$_2$ is ionized by the stripping collisions forming $\approx 20$ keV H$_2^+$. Additionally, stripping of the H beam and dissociative ionization of the H$_2$ can produce $\approx 10$ keV H$^+$.

After the gas cell, the neutrals and resulting ions enter the analyzer region involving two double-focusing, electrostatic cylindrical deflectors in series [10] and a channel electron multiplier (CEM). A hole in the outer plate of the first or lower cylindrical deflector (LCD) allows neutrals to pass through and travel into a neutral detector. The neutral particle current $I_H$, as measured in amperes, is monitored by measuring the secondary negative particle emission from the target inside the neutral detector. The voltages on the LCD and upper cylindrical deflector (UCD) are selected to transmit the 20-keV H$_2^+$ signal ions into the CEM while rejecting any of the 10-keV H$^+$ formed in the gas cell.

We study reaction (1) from the number of H$_2^+$ ions detected in the CEM. Experimentally, we measure the cross section $\sigma_{AD}$ times the relative velocity $v_r$ between the H$^-$ and H beams convolved with the velocity spread of the experiment. This gives the rate coefficient [6]

$$\langle \sigma_{AD} v_r \rangle = \frac{1}{\sigma_{st} N_{He}} \frac{S}{T_a T_g \eta} \frac{e^2}{I_{H^-} I_H} \frac{v_{H^-} v_H}{L \langle \Omega(z) \rangle}. \quad (4)$$

The left-hand-side average is over the experimental energy spread. On the right side, $\sigma_{st}$ is the stripping cross section for H$_2$ on He forming H$_2^+$ [11], $N_{He}$ is the gas cell helium column density, $S$ is the background-subtracted, pressure-corrected H$_2^+$ signal, $T_a$ is the transmittance of the combined LCD-UCD analyzer, $T_g$ is the transmittance of the grid in front of the CEM, $\eta$ is the CEM efficiency, and $v_{H^-}$ and $v_H$ are the velocities of the H$^-$ and H beams, respectively.

## B. Modifications

The present work uses a current meter with a fast response time, enabling us to directly measure the H$^-$ current at each phase in the chopping pattern, which is on the millisecond scale, and monitor it throughout each data run. Thus we are able to measure the anion current when the laser is on, $I_{H^-}^{on}$, over the course of a data run. This is used for $I_{H^-}$ in Eq. (4). We were also able to monitor the anion current with the laser off, $I_{H^-}^{off}$, and determine the attenuation factor

$$f = 1 - \frac{I_{H^-}^{on}}{I_{H^-}^{off}}, \quad (5)$$

which is needed to extract the background-corrected $S$ [6]. This situation is to be contrasted with our previous results [3,6], where, due to equipment limitations, the H$^-$ current was averaged over the H$^-$ chopping cycle and the resulting $\langle I_{H^-}^{chop} \rangle$ was recorded using a slow current meter. As a result, for that work $f$ was not measured during data collection but under simulated data collection conditions, and an average value was used. Additionally, this factor was used to extract $I_{H^-}^{on}$ and $I_{H^-}^{off}$ from $\langle I_{H^-}^{chop} \rangle$.

For the present work we are also using a new calibrated neutral detector in combination with a fast current amplifier to record the H particle current at each phase in the chopping pattern and to monitor it throughout each data run. This modification is described in [6]. Thus, during a data run, we are now able to directly measure $I_H$, which is needed in Eq. (4). In our previous work, the H particle current was also monitored with a fast current amplifier; however, the neutral detector was not designed for absolute measurements. So to analyze those results, using the new detector we measured the H particle current due to photodetachment (PD), $I_H^{PD}$, to determine the neutral-to-anion (nta) ratio

$$f_{nta} = \frac{I_H^{PD}}{I_{H^-}^{off}} \quad (6)$$

under simulated data collection conditions. This factor, combined with the extracted $I_{H^-}^{off}$ discussed above, was then used in [6] to determine $I_H$ for Eq. (4).

We have also installed a BPM immediately before the neutral detector, at a distance of 2055 mm from the first BPM in the interaction region. Turning off the voltage of the LCD allows the H$^-$ beam to pass through the hole in the outer plate of the LCD. We used this additional BPM to measure the position of both the H and H$^-$ beams and verified the alignment of the beams over a much longer lever arm than was previously possible using only the two BPMs in the interaction region. We find that the full angle between the beam axes measured here is in good agreement with that reported in [6].

## C. Pressure corrections

Any H$_2^+$ formed in the gas cell can be destroyed by subsequent collisions with He in either the gas cell or the analyzer region. The resulting products are not transmitted by the electrostatic deflectors into the CEM, thereby reducing the apparent signal and rate coefficient. This small systematic shift in our data was overlooked in our previous work [3,6]. Here

we quantified this minor correction for both our previous and present results.

We measured the H$_2^+$ attenuation using an approach similar to the one we used to determine the He gas cell column density in Refs. [3,6]. Reconfiguring the ion source to produce H$_2^+$ and the apparatus to transmit H$_2^+$ beams, we used the electrostatic quadrupole after the interaction region to direct the beam into a Faraday cup, where we measured the unattenuated H$_2^+$ current $I_{H_2^+}^o$. We then guided the beam through the gas cell and measured the transmitted current, $I_{H_2^+}^o$, on the outer plate of the UCD. With no He in the gas cell, the UCD reading was over 95% of that in the Faraday cup. The measured attenuated data were corrected for this slight difference in the unattenuated current readings.

The H$_2^+$ attenuation as a function of gas density is given by

$$\frac{I_{H_2^+}}{I_{H_2^+}^o} = \exp(-\sigma_d N_{He}), \tag{7}$$

where $\sigma_d$ is the total H$_2^+$ destruction cross section and $N_{He}$ is the helium column density. Following the methodology of [6], the column density can be expressed as

$$N_{He} = \int_{quad} n_{He}(l)dl + \int_{gas\,cell} n_{He}(l)dl + \int_{analyzer} n_{He}(l)dl. \tag{8}$$

Here $n_{He}(l)$ is the helium density, and $dl$ is the infinitesimal path length. Using the same model as [6], we take the pressure to be constant in each of these regions and reexpress Eq. (8) as

$$N_{He} = n_1 l_1 + n_2 l_2 + n_3 l_3. \tag{9}$$

The He density in the quadrupole is $n_1$, and the path length $l_1 = 5.0 \pm 1.0$ cm. In the gas cell the He density is $n_2$, and the path length $l_2 = 78.7 \pm 1.0$ cm. The He density in the analyzer region is $n_3$, and the path length $l_3 = 35.4 \pm 1.0$ cm is the distance that the ions travel before striking the UCD. All uncertainties here and throughout the paper are given at an estimated $1\sigma$ statistical confidence level. The respective densities were calculated from the measured pressures using the ideal gas law at the laboratory temperature, which was stabilized at 293 K for both the work of [3,6] and our new results here. The ratio of the measured pressures in each section were $p_1/p_2 = 0.137 \pm 0.019$ and $p_3/p_2 = 0.105 \pm 0.034$. The uncertainties in these ratios are due to the manufacturer-quoted accuracies of the pressure gauges (10% for $p_1$ and $p_2$ and 30% for $p_3$).

Attenuation data were collected for pressures up to $\approx 4.5 \times 10^{-4}$ Torr and are shown in Fig. 1. From a fit to these data we extracted a cross section of $(2.75 \pm 0.29) \times 10^{-16}$ cm$^2$ at an energy of 10 keV amu$^{-1}$. This estimated uncertainty is due to the error in the attenuated and unattenuated current readings (3% each) and the uncertainty in the He column density (10%). The error in this latter quantity was estimated by adding the uncertainties from each segment $n_i l_i$ of the total column density. The errors in the path lengths and gas densities (i.e., pressures) have been given above.

Collisional destruction of H$_2^+$ has also been studied by Suzuki *et al.* [12], who reported cross sections of various outgoing channels for ion energies from 2 to 8 keV amu$^{-1}$.
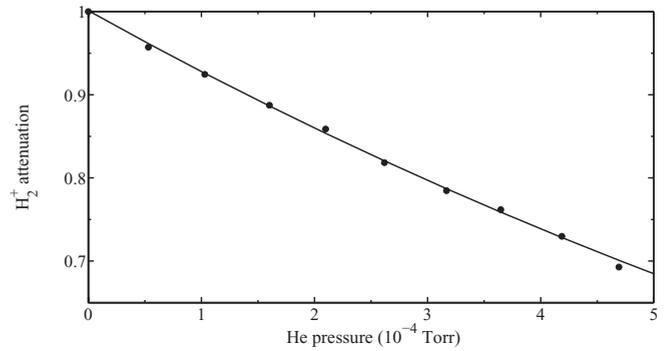


FIG. 1. Attenuation of the H$_2^+$ ion beam as a function of helium gas cell pressure. The circles represent the statistically weighted mean from three sets of measurements. The error bars are smaller than the plotted circles. The line shows the best exponential fit.

We have derived a total destruction cross section by summing the relevant channels in [12]. Those results, shown in Fig. 2, indicate that the cross section is essentially constant between 2 and 8 keV amu$^{-1}$. Our result at 10 keV amu$^{-1}$, also shown in Fig. 2, is in good agreement with this trend.

To determine the expected signal attenuation factor and correct for the H$_2^+$ signal loss we use our measured H$_2^+$ destruction cross section combined with Eq. (7). The appropriate He column density is given by

$$N'_{He} = \tfrac{1}{2} n_2 l_2 + n_3 l'_3, \tag{10}$$

where the factor of 1/2 takes into account that on average the H$_2^+$ ions will be formed in the center of the gas cell and $l'_3 = 57.9 \pm 1.0$ cm is the distance from the end of the gas cell to the CEM mouth. Using these values, we calculate from Eq. (7) that the signal attenuation with $2 \times 10^{-4}$ Torr He in the gas cell is $0.92 \pm 0.01$. The signal must be divided by this factor to correct for the attenuation. This corresponds to an $(8.6 \pm 1.2)\%$ upward shift in the data. The uncertainty in this correction is estimated by propagating through Eq. (7) the quadrature sum of the uncertainties from both $N'_{He}$ in Eq. (10) and $\sigma_d$.
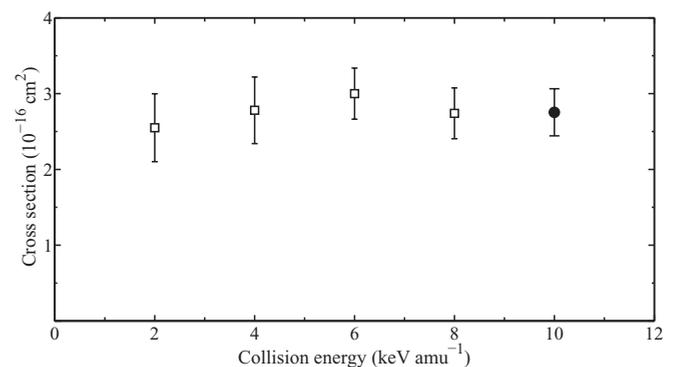


FIG. 2. Experimental cross sections for total H$_2^+$ destruction vs ion beam energy for H$_2^+$ + He. The open squares are the results of [12], while the circle represents our measurement. The error bars for each data set give the total $1\sigma$ experimental uncertainty.

TABLE I. Summary of systematic uncertainties at an estimated $1\sigma$ confidence level. Uncertainties are treated as random sign errors and added in quadrature.

| Source | Error (%) |
|---|---|
| Background subtraction | 5 |
| Anion current | 3 |
| Neutral current | 10 |
| Beam overlap | 3 |
| Total relative errors from above | 12 |
| Stripping cross section | 16 |
| Effects of unknown rovibrational population | 10 |
| Analyzer transmittance | 1 |
| Grid transmittance | 1 |
| CEM detection efficiency | 2 |
| Overlap length | 1 |
| Helium gas cell column density | 7 |
| $H_2^+$ Attenuation | 1 |
| Total systematic uncertainty | 24 |

## III. UNCERTAINTIES

The various systematic uncertainties for the measurement are given in Table I. Values are listed at an estimated $1\sigma$ statistical confidence level. We have grouped them into two sets. The errors listed in the top third of Table I add in quadrature to $\pm 12\%$ for each data point. This represents the relative uncertainty between our old and new data sets and also at different energies within each set. Adding this in quadrature with the remaining uncertainties in the bottom two-thirds of Table I yields the total systematic error of $\pm 24\%$. A detailed discussion is given in [3,6] for the various uncertainties not already discussed here.

## IV. THEORY

### A. Earlier calculations

In our previous work, the AD cross section was calculated using nonlocal resonance theory and considering only the coupling of the $H + H^-$ and $H_2 + e^-$ channels through the lowest metastable $H_2^-$ state of $^2\Sigma_u^+$ symmetry (see [3,8] for details). This state is one of two connected to the $H + H^-$ asymptote (not counting the spin degeneracy). Potential energy curves for both states are shown in Fig. 3. The second state of $^2\Sigma_g^+$ symmetry is repulsive and is usually neglected in the calculations. The validity of this approximation is supported by the very good agreement between our experimental results [3,6] and our nonlocal calculations [3,8] below 1 eV, even after the $\sim 9\%$ pressure correction of the $H_2^+$ signal described in Sec. II C, which was not accounted for in [3,6].

### B. New calculations

We have extended our experimental results to $\sim 5$ eV, entering a regime where AD via the $^2\Sigma_g^+$ state becomes possible. Figure 3 shows that for sufficiently large energies the colliding $H + H^-$ can penetrate into the autodetachment region along the repulsive $^2\Sigma_g^+$ state. This region is defined as the range of internuclear separations $R$ where an electron can
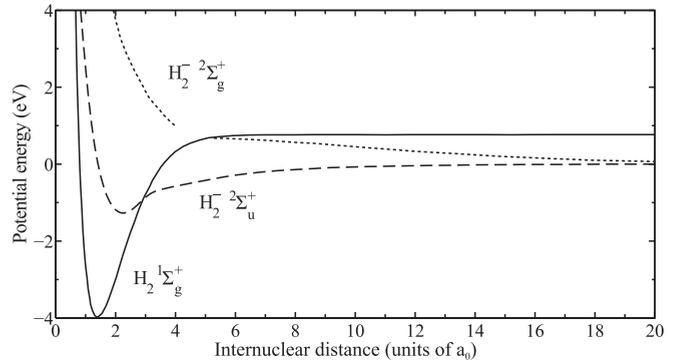


FIG. 3. $H_2^-$ and $H_2$ potential curves vs internuclear distance in units of the Bohr radius $a_0$. The $H_2^-$ attractive $^2\Sigma_u^+$ electronic state is given by the dashed curve [13], and the repulsive $^2\Sigma_g^+$ electronic state is given by the dotted curve constructed using the data of [14,15] below $\sim 4a_0$ and those of [16] above $\sim 5a_0$. The separated atoms limit (SAL) for these two potential energy curves is $H^-(^1S) + H(^2S)$. The solid curve shows the $H_2$ $^1\Sigma_g^+$ electronic state from [17] with a SAL of $H(^2S) + H(^2S)$. The energy difference between the two limits is determined by the H electron affinity energy $E_{EA} = 0.76$ eV [18].

escape the anionic system, i.e., the potential energy curves of the $H_2^-$ system are above those for neutral $H_2$. This occurs for the $^2\Sigma_g^+$ state at $R < 5a_0$, where $a_0$ is the Bohr radius. Particles colliding along this state can penetrate into the autodetachment region for energies $\gtrsim 0.75$ eV motivating calculations for AD via this state.

Due to the different symmetry of the molecular orbitals, the $^2\Sigma_u^+$ and $^2\Sigma_g^+$ contributions to the AD cross section can be calculated separately. Thus we need only carry out new calculations for the $^2\Sigma_g^+$ state. A brief description of our approach is presented below, using atomic units. A more detailed discussion will be given in a future presentation.

Nonlocal resonance theory is explained in detail by [19]. The main idea is as follows. The electronic state $\phi_d$, describing the colliding partners in the $H + H^-$ channel, is diabatically prolonged to small $R$. It is also assumed to be coupled to the $H_2 + e^-$ electronic continuum states $\phi_k$ through the matrix element

$$V_{dk}(R) = \langle \phi_d | H_{el} | \phi_k \rangle,$$

where $H_{el}$ is the electronic Hamiltonian. The nonlocal resonance model is parametrized by three functions: $V_0(R)$, $V_d(R)$, and $V_{dk}(R)$. The potential energy curves for the neutral molecule $V_0(R)$ and for the anion $V_d(R)$ are functions only of $R$. The coupling element $V_{dk}(R)$, however, depends on both $R$ and the momentum of the detached electron $k$.

Once $V_0(R)$, $V_d(R)$, and $V_{dk}(R)$ are known, the electronic dynamics of the system is fully parametrized, and the nuclear dynamics can be treated as a motion in the nonlocal energy-dependent effective potential:

$$V_d(R) + \int V_{dk} \left[ E - \tfrac{1}{2}k^2 - T_N - V_0(R) + i\varepsilon \right]^{-1} V_{dk}^* k\, dk\, d\Omega_k.$$

$T_N$ is the kinetic energy operator for the nuclei, $d\Omega_k$ is the differential solid angle for the outgoing electron, and $\varepsilon$ is the usual positive infinitesimal of scattering theory. We solve the nuclear dynamics and calculate the cross sections using the method of [8].

In order to include $\phi_d$ for the $^2\Sigma_g^+$ state, we have to fix the parameters of the nonlocal resonance model for this state. The proper procedure for calculating these parameters involves extracting the discrete state $\phi_d$ from the continuum $\phi_k$, employing the projection-operator technique. This procedure was followed in [20] for the $^2\Sigma_u^+$ state, and we used it as an input for our calculation [8]. But it is also possible to fix the model parameters by fitting the fixed-nuclei scattering data. We follow this latter procedure here.

To fix the coupling amplitude, we assume the separable form $V_{dk}(R) = g(R)f(k)$, where the $k$ dependence is determined by the Wigner threshold law [21] with an exponential cutoff:

$$f(k) \sim k^{2l+1}e^{-\alpha k^2}, \qquad (11)$$

where $\alpha$ is the cutoff parameter. The angular momentum $l$ value in Eq. (11) is given by the lowest electron partial wave allowed by symmetry (discussed below). The $R$ dependence is determined from the calculated local decay widths $\Gamma(R)$ of [14]. The potential energy curve for the anion $V_d(R)$ is constructed from [14,15] and extended to larger $R$ using the data of [16]. The data for the potential near the crossing of the neutral and anion potential energy curves are missing. Nevertheless, the analytic behavior near the crossing has been discussed in detail by [19]. With this knowledge, the potential energy curve can be interpolated through the crossing as has been done before for hydrogen halides [22]. The actual shape of the $V_d(R)$ and $V_0(R)$ crossing is modified by the interaction of the electron scattering continuum with the threshold behavior given by Eq. (11). $V_0$ is from [17].

The decay of the odd-symmetry anion $^2\Sigma_u^+$ state to the even neutral $^1\Sigma_g^+$ state is possible only through release of an electron with odd angular momentum. In [3,8] we considered only $l = 1$ ($p$-wave scattering) since the calculations of [23] show that the next allowed $l = 3$ contribution is suppressed by almost two orders of magnitude for the energy range of interest. For the anion $^2\Sigma_g^+$ state decaying to the neutral $^1\Sigma_g^+$ state, the symmetry remains unchanged, requiring release of an electron with even angular momentum. Here we considered only $l = 0$ ($s$-wave scattering). In each case, as Eq. (11) shows, $V_{dk}$ is strongly suppressed for higher angular momenta at the $k < 1$ values in our experimental results.

The anion $^2\Sigma_g^+$ state can also decay to the first excited $^3\Sigma_u^+$ state of $H_2$. These states are both repulsive and lie very close together. This decay, however, requires an odd value for $l$. With $l = 1$ and $k < 1$, $f(k)$, and hence $V_{dk}$, is strongly suppressed compared to the $^2\Sigma_g^+$ to $^1\Sigma_g^+$ decay channel with $l = 0$. The effect from the transition between repulsive states is thus expected to be small at low energies and was not included here.

Once the model parameters are fixed, $\sigma_{AD}$ can be calculated using the methods described in [8]. Figure 4 shows our results. As expected from the previous good agreement of our experimental and theoretical results, the new contribution is small and notable only for $E_r \gtrsim 0.75$ eV. This is the threshold where the colliding particles overcome the barrier in the repulsive interaction potential and penetrate into the autodetachment region.
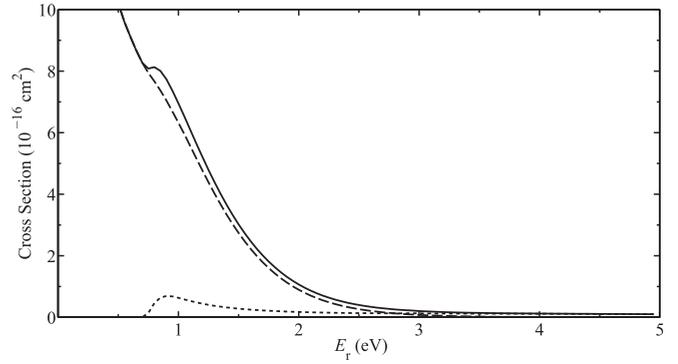


FIG. 4. Theoretical cross section for $H^- + H \rightarrow H_2 + e^-$ as a function of the relative collision energy $E_r$. The dashed curve shows the results via the attractive $H_2^-$ $^2\Sigma_u^+$ state, the dotted curve shows the repulsive $H_2^-$ $^2\Sigma_g^+$ state, and the solid curve shows the sum of the two.

Both the $^2\Sigma_u^+$ and $^2\Sigma_g^+$ contributions decay rapidly to zero for energies above $\sim$1 eV. This is due to the competing process of collisional detachment,

$$H^- + H \rightarrow H + H + e^-, \qquad (12)$$
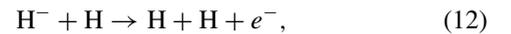
which opens up for $E_r = 0.76$ eV and wins at higher energies. This is discussed in Sec. VI from the point of view of general energy-conservation arguments.

### C. Contributions from quasibound $H_2$ states

At high angular momentum ($J > 10$), the colliding $H^-$ and H systems can autodetach into quasibound $H_2$. These states, sometimes referred to as orbiting or shape resonances, lie above the separated-atoms limit for H + H. Such high $J$ levels, temporarily stabilized by the centrifugal barrier, will eventually dissociate spontaneously and are therefore generally not considered in AD cross-section calculations. However, the lifetime for all but a few of these resonances well exceeds the flight time from the interaction region to the gas cell, and so most are expected to contribute to the experimental signal.

The $H_2$ flight time from the interaction region to the gas cell is $(737 \pm 640)$ ns. The mean is the center-to-center distance, the upper limit is from the start of the interaction region to the end of the gas cell, and the lower limit is from the end of the interaction region to the start of the gas cell. Quasibound $H_2$ (i.e., in high $J$ levels) can strip in the He gas cell and will form $H_2^+$ in similarly high $J$ levels. As the $H_2^+$ potential supports stable rovibrational levels up to $J = 35$, we assume that any such $H_2^+$ formed will be stable and will reach the detector.

In order to compare to our measured results, we have added the contribution of these quasibound $H_2$ states to our calculations for AD via the $^2\Sigma_u^+$ state. So as to mimic the range of experimental lifetimes, we have investigated the effect of cutting out states with lifetimes less than 100, 700, and 1400 ns and found no significant differences. In the end we included contributions from all resonances with lifetimes longer than 700 ns. The contribution of these states is of comparable size to the $^2\Sigma_g^+$ state contribution. The effect of these resonances for AD via the $^2\Sigma_g^+$ state has not been considered as that would
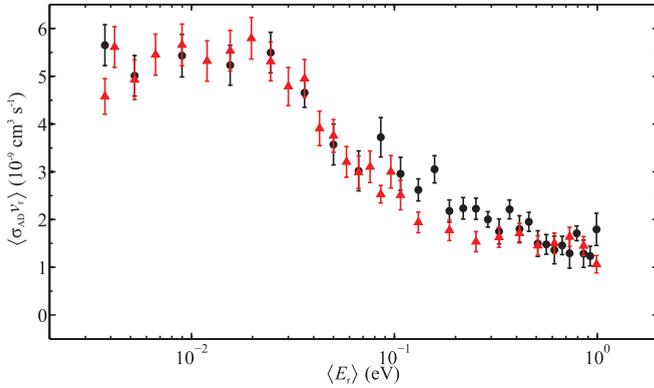
FIG. 5. (Color) Experimental rate coefficient $\langle \sigma_{AD} v_r \rangle$ as a function of the collision energy $\langle E_r \rangle$. The black circles show our new results, and the red triangles show our previous results from [3,6] corrected for the $H_2^+$ attenuation. Although our new results extend up to $\langle E_r \rangle \leqslant 4.83$ eV, here we show only up to the maximum $\langle E_r \rangle$ of our previous results for comparison. The error bars show the $1\sigma$ statistical uncertainties. There is an additional $\pm 12\%$ relative systematic error on each data point that is not shown.

be a small correction to an already small contribution. Last, we note that the significance of these resonances for molecular hydrogen formation in plasma environments will depend on whether the states can relax to stable states of $H_2$ before they dissociate by tunneling.

## V. RESULTS

Relative energies $E_r$ are controlled by varying the potential of the floating cell $U_f$. In [3,6] data were collected for $E_r \leqslant 1$ eV ($|U_f| \leqslant 281$ V). Here we have extended the energy range to $E_r \leqslant 4.83$ eV ($|U_f| \leqslant 621$ V). Data are collected by stepping $U_f$ in voltage. The present work uses voltage ranges smaller than our earlier measurements. For $|U_f| \leqslant 441$ V, $U_f$ was scanned across 60 V ranges in 10 V steps, and for $|U_f| \geqslant 441$ V the scanning was across 120 V ranges in 20 V steps.

Our measured rate coefficients for reaction (1) are plotted in Fig. 5 as a function of average collision energy $\langle E_r \rangle \leqslant 1.0$ eV. The black circles represent our new results, and the red triangles represent our previous work. Both have been corrected for the attenuation of the $H_2^+$ ions. The error bars on each data point display the $1\sigma$ statistical uncertainty. There is an additional $\pm 12\%$ relative systematic error on each data point that is not shown. The good agreement between our new and previous results indicates that there were no hidden systematic errors due to our previous inability to measure and monitor $f$ and $f_{nta}$ during data acquisition.

A final potential source of systematic error that we investigated was to verify the linearity of the gas-stripping method used to convert the product $H_2$ molecules into the measured $H_2^+$ signal. Here we measured the AD rate coefficient as a function of helium gas cell pressure for $(1-3) \times 10^{-4}$ Torr. Table II the results of these AD measurements at $\langle E_r \rangle = 16$ meV versus pressure. Taking into account the attenuation of the $H_2^+$ signal ions, to within the uncertainties the data show no dependence on gas cell pressure.

Given the good agreement between our results in [3,6] and our new data, we have merged them together using a statistically weighted averaging method. We also included our pressure-test results in this average. The $1\sigma$ counting statistics of each data point were used for the weighting. All data sets were also measured on the same relative energy grid. Figures 6 and 7 present the averaged data for $\langle E_r \rangle \leqslant 1$ eV plus the new data we have collected for $1.0$ eV $\leqslant \langle E_r \rangle \leqslant 4.83$ eV. Also shown are the cross-section calculations of [3,8], supplemented by our new theoretical work here, multiplied by $v_r$, and convolved with the experimental energy spread. Figure 7 shows the theoretical results with and without the effects of the $H_2$ orbiting resonances included. As is clear from Figs. 6 and 7, we find good agreement with theory throughout the measured energy range. The contribution due to orbiting resonances of $H_2$ can also be seen in Fig. 7, as the experimental data are shifted to slightly higher energy compared to the calculations which do not include these resonances.

## VI. DISCUSSION

The good agreement that we find here both with our previous results and with our updated theory strengthens our confidence that theory and experiment have finally converged for reaction (1). Including AD via the repulsive $^2\Sigma_g^+$ state increases the cross section by an amount smaller than we are currently able to measure experimentally. The resulting theoretical thermal rate coefficient is only 1.3% larger than that for only the attractive state at temperatures of 4000 K, 3.5% at 8000 K, and 4.4% larger at 10 000 K. These are significantly smaller than the $\approx 25\%$ experimental accuracy with which we have been able to benchmark theory. Hence, we continue to recommend the thermal rate coefficient of [3] for modeling plasma temperatures below $10^4$ K.

Additionally, our results continue to imply that the reason for the discrepancy seen with the results of [4] lies in the data of [7] used for normalization. This is further supported by the theoretical AD work on hydrogen halides of [24]. They used the same theoretical approach as we do here and found systematically higher AD rate coefficients than the

TABLE II. Rate coefficient results at $\langle E_r \rangle = 16$ meV versus helium gas cell pressure. Our theoretical results are also shown for comparison.

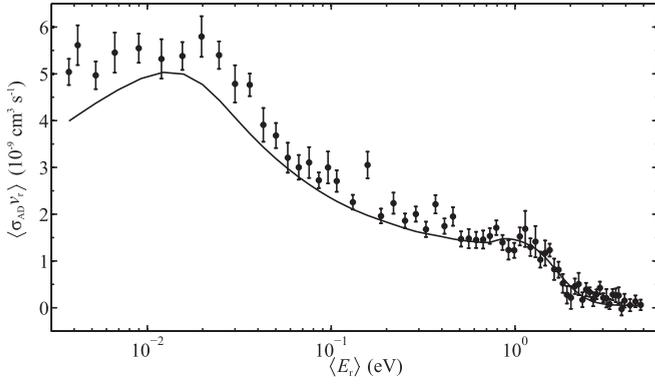| Pressure ($10^{-4}$ Torr) | Rate Coefficient ($10^{-9}$ cm$^3$ s$^{-1}$) | | |
|---|---|---|---|
| | Value | Statistical uncertainty | Relative uncertainty |
| 1.0 | 5.6 | $\pm 0.5$ | $\pm 0.7$ |
| 2.0 | 5.2 | $\pm 0.4$ | $\pm 0.6$ |
| 3.0 | 5.2 | $\pm 0.4$ | $\pm 0.6$ |
| Theory | 5.0 | | |

FIG. 6. The circles show the statistically weighted mean of the experimental rate coefficients $\langle \sigma_{AD} v_r \rangle$ from our previous [3,6] and current work as a function of the collision energy $\langle E_r \rangle$ (see text). For $\langle E_r \rangle \geqslant 1.0$ eV the data are solely from the current measurement. The error bars represent the $1\sigma$ statistical uncertainties. The solid line is from the cross-section calculations of [3,8], supplemented by our new theoretical work here, multiplied by $v_r$, and convolved with our experimental energy spread. The effects of the $H_2$ orbiting resonances have been included in the calculations shown here.

experimental work of [7]. It appears to us that a remeasurement of reaction (2) using a technique different from that of [7] is clearly called for to resolve this dilemma.

Our results also verify the predictions of [8] and our new theoretical work here that the AD cross section for reaction (1) should decrease to essentially insignificant values for $E_r \gtrsim 2$ eV, as shown in Fig. 6. A simplified adiabatic description of the AD reaction can provide good insight into the physics behind this prediction. We consider here only the $^2\Sigma_u^+$ symmetry. Similar arguments can also be given for the $^2\Sigma_g^+$ state.

Initially, the H⁻ and H approach one another along the attractive $^2\Sigma_u^+$ electronic state. This state crosses into the autodetachment region at $R \sim 3a_0$. Adiabatic theory dictates that the system remains electronically in the ground state. Inside the autodetachment region the ground state is the $^1\Sigma_g^+$ state of neutral $H_2$ plus a free electron with zero kinetic energy. Conservation of energy requires that the final state energy equals that initially available
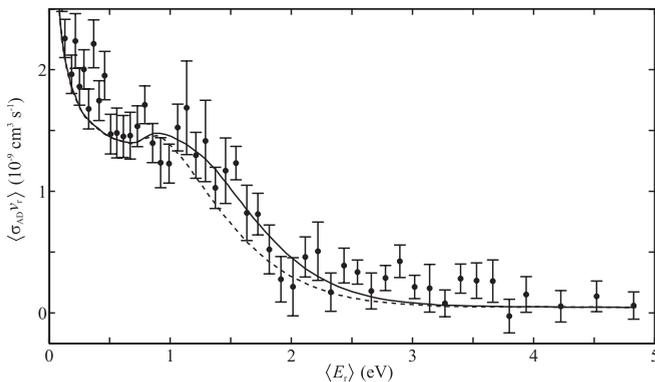
$$E_v = E_r + D_0 - E_{EA}. \tag{13}$$



FIG. 7. Same as Fig. 6, but on a linear scale. The dotted curve shows the calculations without the effects of the $H_2$ orbiting resonances included.

Here $E_v$ is the excitation energy of the vibrational level $v$ formed in the process, $D_0$ is the 4.48-eV dissociation energy gained by formation of $H_2$ in the $v = 0$ vibrational and $J = 0$ rotational level [25], and $E_{EA} = 0.76$ eV is the electron affinity required to neutralize the H⁻ and form H [18]. For $E_r > E_{EA}$, the system lies in the dissociation continuum ($E_v > D_0$), resulting in the formation of H + H + e⁻ and not $H_2$ + e⁻.

In reality the AD process is not exactly adiabatic. This is manifested by the release of an electron with a nonzero kinetic energy $E_e$, and we can rewrite (13) as

$$E_v + E_e = E_r + D_0 - E_{EA}. \tag{14}$$

The nonadiabatic exchange of energy between the electron and protons is weak though; detached electrons do not have a large kinetic energy. Our full calculations for the $^2\Sigma_u^+$ state [8] show that only a negligible amount of electrons can have energy above $\sim$1.5 eV. Taking into account that the largest possible value of $E_r$ will occur for $E_v = D_0$, this leads to the prediction that the AD process will cease for $E_r \gtrsim E_{EA} + 1.5$ eV. For reaction (1), this corresponds to $E_r \gtrsim 2.26$ eV. A similar argument has been suggested for the decrease in the cross section for protonium formation in collisions of antiprotons with hydrogen atoms (see [26] for a review). Note that we have ignored the insignificant kinetic energy of the final $H_2$ molecule $E_{H_2}$, as conservation of momentum gives $E_{H_2} = (m_e/m_{H_2})E_e \ll E_e$.

Continuing the protonium analogy, one would expect a sharp decrease in $\sigma_{AD}$ immediately after the collisional detachment threshold at $E_r = 0.76$ eV. In the H⁻ + H collision, the drop in the cross section occurs at higher energies. This is related to the threshold law given by Eq. (11) with $l = 1$ for the dominant ungerade channel. As a result, the coupling $V_{dk}$ vanishes for zero detached electron energy and rises smoothly as the energy increases. The electron energy in Eq. (14) thus cannot be exactly zero, but remains relatively small. The smooth decrease in $\sigma_{AD}$ above 1 eV, confirmed by the present experiment, thus provides a good test of the theoretical description of the electron release amplitude.

Last, the decrease of the AD cross section is indeed slightly weakened by positive contributions of the $^2\Sigma_g^+$ state, as shown in Fig. 4, and orbiting resonances, as seen in Fig. 7. However, the decreasing trend above 1 eV, controlled by $V_{dk}$, is still dominant (e.g., Fig. 6).

## VII. SUMMARY

We have modified the experimental methods used in [3,5,6] to measure reaction (1) up to $E_r \leqslant 4.83$ eV. Additionally, we have performed several modifications to better control potential systematic errors. We find good agreement between our previous and new data sets. To within the experimental uncertainties, we also continue to find good agreement with the calculations of [3,8], which have been extended here to include contributions from the repulsive $^2\Sigma_g^+$ $H_2^-$ state and for the effects on the experimental results due to orbiting resonances of $H_2$ for $E_r \geqslant 0.76$ eV. In particular, we confirm the predictions of [8] that this reaction turns off for $E_r \gtrsim 2$ eV. Similar behavior has been predicted for the formation of protonium from collisions of antiprotons and hydrogen atoms [26].

## ACKNOWLEDGMENTS

[1] S. C. Glover, D. W. Savin, and A.-K. Jappsen, Astrophys. J. **640**, 2 (2006).

[2] S. C. O. Glover and T. Abel, Mon. Not. R. Astron. Soc. **388**, 4 (2008).

[3] H. Kreckel, H. Bruhns, M. Čížek, S. C. O. Glover, K. A. Miller, X. Urbain, and D. W. Savin, Science **329**, 69 (2010).

[4] O. Martinez Jr., Z. Yang, N. B. Bettes, T. P. Snow, and V. M. Bierbaum, Astrophys. J. **705**, L172 (2009).

[5] H. Bruhns *et al.*, Rev. Sci. Instrum. **81**, 013112 (2010).

[6] H. Bruhns, H. Kreckel, K. A. Miller, X. Urbain, and D. W. Savin, Phys. Rev. A **82**, 042708 (2010).

[7] C. J. Howard, F. C. Fehsenfeld, and M. McFarland, J. Chem. Phys. **60**, 5086 (1974).

[8] M. Čížek, J. Horáček, and W. Domcke, J. Phys. B **31**, 2571 (1998).

[9] R. A. Phaneuf, C. C. Havener, G. H. Dunn, and A. Müller, Rep. Prog. Phys. **62**, 1143 (1999).

[10] H. Kreckel, H. Bruhns, K. A. Miller, E. Wåhlin, A. Davis, S. Höckh, and D. W. Savin, Rev. Sci. Instrum. **81**, 063304 (2010).

[11] R. Browning, C. J. Latimer, and H. B. Gilbody, J. Phys. B **3**, 667 (1970).

[12] Y. Suzuki, T. Kaneko, M. Tomita, and M. Sakisaka, Phys. Soc. Jpn. **55**, 3037 (1986).

[13] J. Senekowitsch, P. Rosmus, W. Domcke, and H.-J. Werner, Chem. Phys. Lett. **111**, 211 (1984).

[14] D. T. Stibbe and J. Tennyson, J. Phys. B **31**, 815 (1998).

[15] D. T. Stibbe and J. Tennyson, Chem. Phys. Lett. **308**, 532 (1999).

[16] J. N. Bardsley and J. M. Wadehra, Phys. Rev. A **20**, 1398 (1979).

[17] L. Wolniewicz, J. Chem. Phys. **103**, 1792 (1995).

[18] J. Horáček, M. Čížek, K. Houfek, P. Kolorenč, and W. Domcke, Phys. Rev. A **70**, 052712 (2004).

[19] W. Domcke, Phys. Rep. **208**, 97 (1991).

[20] M. Berman, C. Mundel, and W. Domcke, Phys. Rev. A **31**, 641 (1985).

[21] E. P. Wigner, Phys. Rev. **73**, 1002 (1948).

[22] M. Čížek, J. Horáček, and W. Domcke, Phys. Rev. A **60**, 2873 (1999).

[23] M. Berman, C. Mündel, and W. Domcke, Phys. Rev. A **31**, 641 (1985).

[24] K. Houfek, M. Čížek, and J. Horáček, Phys. Rev. A **66**, 062702 (2002).

[25] Y. P. Zhang, C. H. Cheng, J. T. Kim, J. Stanojevic, and E. E. Eyler, Phys. Rev. Lett. **92**, 203003 (2004).

[26] J. S. Cohen, Rep. Prog. Phys. **67**, 1769 (2004).